Hu, Sha; Ilter, Mehmet C.; Wang, Hao

Near-Field Beamforming for Large Intelligent Surfaces

Published in:
2022 IEEE 33rd Annual International Symposium on Personal, Indoor and Mobile Radio Communications, PIMRC 2022

DOI:
10.1109/PIMRC54779.2022.9977582

Published: 01/01/2022

Document Version
Peer-reviewed accepted author manuscript, also known as Final accepted manuscript or Post-print

Please cite the original version:
Hu, S., Ilter, M. C., & Wang, H. (2022). Near-Field Beamforming for Large Intelligent Surfaces. In *2022 IEEE 33rd Annual International Symposium on Personal, Indoor and Mobile Radio Communications, PIMRC 2022* (pp. 1367-1373). (IEEE International Symposium on Personal, Indoor and Mobile Radio Communications; Vol. 2022-September). IEEE. https://doi.org/10.1109/PIMRC54779.2022.9977582

Near-Field Beamforming for Large Intelligent Surfaces

Sha Hu[†], Mehmet C. Ilter[*†] and Hao Wang[‡]
[†]Lund Research Center, Huawei Technologies Sweden AB, Sweden
[‡]Huawei Technologies Co., Ltd, Beijing, China
[*]Dept. of Signal Processing and Acoustics, Aalto University, Espoo, Finland
{hu.sha, hunter.wanghao}@huawei.com, mehmet.ilter@aalto.fi

***Abstract*—In this paper, we propose a novel near-field beamforming (BF) design with a Large Intelligent Surface (LIS) that is implemented as a discretized 2D-array. We first investigate the definitions of the near-field and far-field regions, and determine the Fraunhofer distance of the LIS, which scales up linearly in the surface-area of the LIS. Hence, a user-equipment (UE) can enter the near-field of a LIS in practice. In addition to Fraunhofer distance, we further derive the Fresnel near-field region where both amplitude and angle variations are negligible, as long as the distance from the UE to the LIS is larger than a threshold, which only scales up linearly in the diameter of LIS. Therefore, in the majority region of near-field, only phase variations worsen the the quality of received signal and result in significant array-gain losses. Motivated by this observation, we further propose a two-step near-field BF design that can effectively recover the array-gain losses in Fresnel near-field, and is fully compatible with a conventional far-field BF.**

I. Introduction

With the featured sixth generation (6G) wireless networks, novel architectures and network elements have been introduced to the existing deployments. Those additions require engineers to redesign network infrastructures and revisit the fundamentals of wireless communication [1]. Recently, the concept of Large Intelligent Surface (LIS) [2]–[4], as an evolution of massive multi-input multi-output (MIMO) system, arises in wireless system design, which introduces substantial gains in signal-transmission and terminal-positioning. Later on, similar concepts including reflection intelligent surface (RIS), intelligent reflection surface (IRS), and holographic MIMO [5]–[8] have also been introduced and gain extensive interests.

In practice, LIS (and other intelligent surfaces) can be implemented in a discretized form based on optimal sampling [2], which is close to an extremely large antenna array (ELAA), whose superior performance of spectral and energy efficiencies have been illustrated with proper network configurations [9]. An important aspect of applying LIS is the design of a suitable beamforming (BF) scheme. Unlike a conventional multi-input multi-output (MIMO) system that directs its beams towards a certain direction, LIS can direct the transmitted radio signal towards a point in a three-dimensional (3D) space. This property has stimulated extensive interests in applying LIS for applications such as wireless energy-transferring [7].

In general, radio-wave propagation is classified into two regions, near-field and far-field. When an antenna radiates a signal in free-space, the field-distribution is uniquely determined by Maxwell's equations, and the characterise of propagation can be different. In far-field, variations of amplitude, angle, and phase are all negligible and path-loss effect is dominant in determining received signal strength. While in near-field, there are noticeable amplitude, angle, and phase variations depending on the distance from a user-equipment (UE) to the antenna-surface [10]. The distance that splits the near-field and the far-field is called the Fraunhofer distance, which limits the phase variations to be less than $\pi/8$. Further, the near-field can be split into reactive and radiative Fresnel regions. The reactive near-field is quite close to the antenna-surface, whose boundary is considered to be $\lambda/(2\pi)$ where λ is the wavelength, and there are strong inductive and capacitive effects from the currents and charges in the antenna. The Fresnel near-field, on the other hand, covers the majority part of near-field spanning by the distance from $\lambda/(2\pi)$ out to the Fraunhofer distance.

With LIS, the definitions of the near and far fields are slightly different from conventional concepts. When considering a single antenna-element on the LIS, the far-field assumption holds in practice whenever a UE is a few wavelengths away. However, the transmitted signals from different antenna-elements reaching the UE can yield distinctive propagation properties even when the UE is relatively far away from the LIS. In which case, the planar-wave assumption dose not hold, and the received signals are close to spherical waves, which means that the UE enters the near-field of the LIS. From this perspective, it is equivalently to view the LIS as an aperture-antenna when considering near-field and far-field regions. However, with a conventional aperture-antenna the entire physical antenna is treated as a whole, but with LIS each antenna-element can be controlled separately, and the near-field BF can be designed to resolve those impacts.

Although near-field BF has been considered in literature [5], [6], [11]–[14], to our best knowledge, it has not been considered from a practical implementation perspective that cooperates with the existing far-field BF. For instance, in [11], the near-field BF vector for a microphone-array in an acoustic system is derived to be equal to the signal propagation vector, which is however, unknown at the transmitter. In [5] and [6], the near-field BF is designed for RIS that cooperates with a

next-generation NodeB (gNB), which shows that the optimal BF weights depend on the distances among the gNB, RIS, and UE. Nevertheless, the design in [5] uses an estimate of distance measured from sensing, while in [6] the BF vector utilizes a codebook based approach with assistance from the UE. In these methods, detailed analysis of the near-field and the far-field regions, and how phases, amplitude, and angles can change in different regions are not elaborated. Further, the insight that the near-field BF can be effectively designed and cooperate with the existing far-field BF scheme is lacking.

In this paper, we propose a novel near-field BF with LIS from a practical perspective. We first derive the Fraunhofer distance that splits the near-field and far-field regions of the LIS, and then derive another distance that determines the Fresnel near-field region. Enlightened by the fact that only phase variations in the Fresnel region worsen the received signal strength, we further propose a two-step methodology to compensate those variations. More specifically, the first BF step follows a conventional far-field BF scheme, which equivalently adjusts the LIS-array such that the UE is transferred to its boresight. Secondly, a further near-field BF scheme compensates the remaining phase variations, which is different from conventional discrete Fourier transform (DFT) beams. Simulation results show that dramatical losses of array-gains can be observed when UE enters the near-field of a LIS, which however, can be effectively recovered with the proposed near-field BF scheme.

II. Near-Field Regions of LIS

To derive the near-field region of LIS, we assume a UE with a single receiving-antenna and under a perfect line-of-sight (LoS) scenario. This is essentially because that when a UE is equipped with an antenna-array for receiving, it is typically of a small size such as 2×2 or 4×4. Therefore, the propagation differences among these receiving-antennas are negligible, and the derived near-field impacts are identical to all receiving-antennas. Once these near-field impacts are effectively compensated at the transmitting LIS, the received signals can be regarded as planner waves when reaching the UE, and the UE can apply a conventional far-field BF for receiving. When the UE is also equipped with a LIS, the impacts from the receiving-LIS should also be considered, which is out the scope of this paper and subjected to future studies. Nevertheless, due to the reciprocity between the transmitter and the receiver, the similar analysis in essence can apply.

A. Near-field Definition with LIS

We consider a two-dimensional (2D) LIS-array which has $M\times N$ antenna-elements[1] where two adjacent antenna-elements are separated from each other with a half-wavelength $\lambda/2$. An illustration is depicted in Fig. 1. Without loss of generality, we assume the LIS-array is located on the $x-y$ plane and centred at the origin point $(0,0,0)$. The coordinates of the (m,n)th element, i.e. an antenna-element located

[1]Other shapes such as a disk-LIS or even 3D-LIS [3] can follow similar analysis, and so are the cases when the antenna-spacing is different from $\lambda/2$.

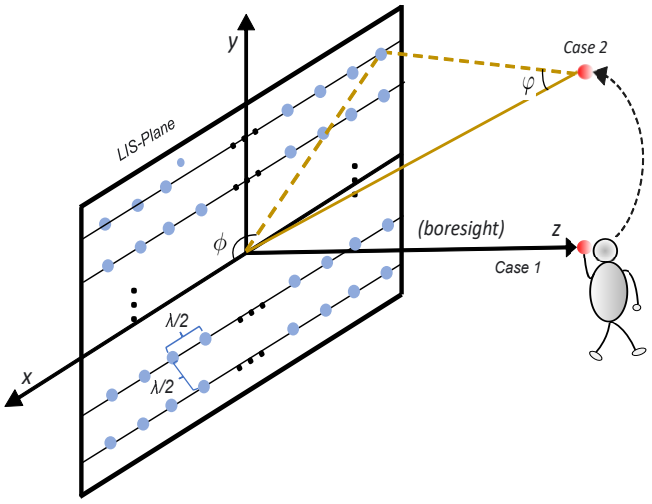

Fig. 1: An illustration of the LIS transmission under a LoS scenario for two difference cases. *Case-1*: a UE is located on the z-axis which is aligned with the boresight of the LIS-array; *Case-2*: a UE is located off the boresight with an elevation angle φ and an azimuth angle ϕ.

on the mth row and the nth column of the LIS-array, are $\left(\left(m-\frac{M}{2}-\frac{1}{2}\right)\frac{\lambda}{2},\left(n-\frac{N}{2}-\frac{1}{2}\right)\frac{\lambda}{2},0\right)$, where $1\le m\le M$, $1\le n\le N$, and both M and N are even integers.

Further, the radius of LIS is defined as

$$D=\frac{\lambda}{4}\sqrt{M^2+N^2}, \tag{1}$$

and the largest distance between two antenna-elements, which are those two at corners on the same diagonal-line, equals

$$\tilde{D}=\frac{\lambda}{2}\sqrt{(M-1)^2+(N-1)^2}. \tag{2}$$

Furthermore, a UE is assumed to be located on $(x,\,y,\,d)$, and without loss of generality, the following mild conditions hold

$$\begin{aligned} d &\gg \lambda \\ M,N &\gg 1. \end{aligned} \tag{3}$$

These conditions indicate that the UE is reasonably far away from the LIS, and the LIS-array is relatively large.

In what follows we consider two different scenarios that are referred to as *Case-1* and *Case-2*:

- For *Case-1*, a UE is located on the boresight of the LIS.
- For *Case-2*, a UE can be arbitrarily located.

With a perfect far-field BF, the transmitting angles in azimuth and elevation directions are aligned, and the UE can be treated as being located on the boresight of LIS, which is the *Case-1*. However, when the UE enters the near-field of LIS, the array-gain can be rapidly decreased. With the *Case-2*, the near-field impacts can be significantly enlarged when the UE is away from the boresight. In the remaining analysis, we always treat *Case-1* firstly, and then generalize the results to the *Case-2*.

1) Case 1: In this case, the UE is located on the boresight of the LIS with coordinates $(0,0,d)$. The shortest and longest distances are denoted as d_1 and d_2, respectively, which

correspond to antenna-elements that are the closest and the farthest to the origin point $(0,0,0)$. They can be computed as

$$d_1 = \sqrt{\frac{\lambda^2}{16} + \frac{\lambda^2}{16} + d^2} = \sqrt{\frac{\lambda^2}{8} + d^2} \approx d, \tag{4}$$

and

$$\begin{aligned} d_2 &= \sqrt{\left(\frac{M}{2} - \frac{1}{2}\right)^2 \frac{\lambda^2}{4} + \left(\frac{N}{2} - \frac{1}{2}\right)^2 \frac{\lambda^2}{4} + d^2} \\ &= \sqrt{\frac{\tilde{D}^2}{4} + d^2}. \end{aligned} \tag{5}$$

The approximation in (4) follows from (3). The ratio between d_1 and d_2 can then be approximated as

$$\frac{d_2}{d_1} \approx \frac{\sqrt{\frac{\tilde{D}^2}{4} + d^2}}{d} \approx 1 + \frac{\tilde{D}^2}{8d^2}, \tag{6}$$

by applying

$$\sqrt{1 + x^2} \approx 1 + \frac{x^2}{2}, \tag{7}$$

which holds when x is sufficiently small, i.e., when $\tilde{D}/(2d)$ in (6) is sufficiently small.

Property 1. *The Fraunhofer distance equals $d_{F,1} = 2\tilde{D}^2/\lambda$ with the Case 1, which defines the boundary of the near-field and far-field regions of the LIS.*

Proof. Utilizing the definition with an aperture-antenna where the Fraunhofer distance is defined for the largest phase-variation to be limited by $\pi/8$, see e.g., [10], it results from (6) that

$$\frac{2\pi}{\lambda}(d_2 - d_1) = \frac{\pi \tilde{D}^2 d_1}{4\lambda d^2} \approx \frac{\pi \tilde{D}^2}{4\lambda d} \leq \frac{\pi}{8}, \tag{8}$$

and hence $d \geq 2\tilde{D}^2/\lambda \triangleq d_{F,1}$. ■

One interesting observation from Property 1 is that $d_{F,1}$ increases quadratically with respect to M and N. When $M = N$, the surface-area of LIS equals $\mathcal{A} = N^2\lambda^2/4$, and it holds that

$$d_{F,1} = (N-1)^2\lambda \approx \frac{4\mathcal{A}}{\lambda}, \tag{9}$$

which linearly increases in the surface-area of the LIS, and decreases in the wavelength λ.

Example 1. *When $\lambda = 5$cm (at a carrier-frequency of 6GHz) and $M = N = 32$, from (9) it holds that $d_{F,1} \approx 48$m, while for $M = N = 64$, $d_{F,1} \approx 198$m. In both cases, the near-field regions are not small, especially for indoor deployments of LIS.*

Although the Fraunhofer distance in Property 1 aligns with the definition of a conventional aperture-antenna whose diameter is $\tilde{D}$, this is under the assumption that the UE is located on the boresight. We will show in the next that with the *Case-2* the near-field region can be significantly enlarged when the UE moves away from the boresight. This indicates that the chance for a UE to enter the near-field region of LIS can be high in practice.

2) Case 2: To continue with the *Case-2*, we first state the Property 2.

Property 2. *The largest phase-variation for an arbitrary UE location is $2\pi\tilde{D}/\lambda$.*

Proof. Seen from Fig. 1 and using the triangle inequality, the distance difference from the UE to any two antenna-elements on the LIS is no larger than $\tilde{D}$, and hence, the largest phase variation is $2\pi\tilde{D}/\lambda$. ■

Note that the largest phase variation only occurs when a UE is infinitely close to the LIS-plane, and such a variation is independent from the distance d. Therefore, Property 2 only shows the theoretical limit. To illustrate the idea better, we consider an example below as a specific instance of *Case-2* for analysing the near-field region.

Example 2. *A UE is located at $\left(\frac{(1-M)\lambda}{4}, \frac{(N-1)\lambda}{4}, d\right)$. That is, the UE is on top of the antenna-element at the upper-right corner in Fig. 1, such that the line connects the antenna-element and the UE is perpendicular to the LIS-plane. Such a case could result from imperfect far-field BF so that the UE is slightly deviated to the boresight.*

With the Example 2, the Fraunhofer distance can be recalculated similar to the *Case 1*. In this case the shortest distance is $d_1 = d$, and the longest one is

$$d_2 = \sqrt{\tilde{D}^2 + d^2}. \tag{10}$$

Thusly, as long as $\tilde{D}/d$ is small, the distance ratio turns into

$$\frac{d_2}{d_1} \approx \sqrt{1 + \frac{\tilde{D}^2}{d^2}} \approx 1 + \frac{\tilde{D}^2}{2d^2}. \tag{11}$$

Property 3. *The Fraunhofer distance of Example 2 with Case-2 is $d_{F,2} = 8\tilde{D}^2/\lambda$, which is four times as large as $d_{F,1}$.*

Proof. Similar to Property 1, for the largest phase-variation to be limited to $\frac{\pi}{8}$, from (11) it holds that

$$\frac{2\pi}{\lambda}(d_2 - d_1) = \frac{\pi \tilde{D}^2}{\lambda d} \leq \frac{\pi}{8}, \tag{12}$$

which shows $d \geq 8\tilde{D}^2/\lambda \triangleq d_{F,2}$. ■

Property 3 shows that when the UE is away from the boresight, the near-field region can be significantly enlarged. This implies that it is important to consider the near-field impacts with LIS systems in practical scenarios.

B. Negligible Amplitude and Angle Variations

So far only phase variations are considered, and there are two other important aspects in the BF, which are amplitude and angle variations. In fact, those are negligible in the Fresnel near-field region, as stated in Property 4.

Property 4. *When the distance $d \gg \tilde{D}$, which is proportional to the wavelength λ, the maximal amplitude and angle variations are small and negligible.*

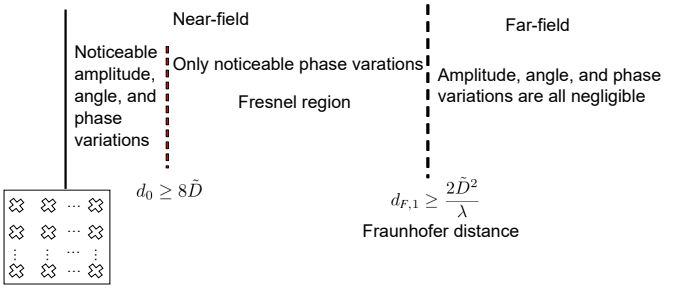

Fig. 2: The near-field and far-field regions of an $M \times N$ LIS-array, when UE is located on the boresight.

Proof. As known, the amplitude of the received signal changes inversely proportional to d^2 or even higher-order in some scenarios. However, from both (6) and (11), it can be seen that in order to make the distance variations small, it is sufficient to have $d \gg \tilde{D}$.

Further, seen from the UE, the largest variation of AoA, assuming to be θ, with the *Case 1* equals

$$\cos\theta = \frac{d_1}{d_2} \approx 1 - \frac{\tilde{D}^2}{8d^2}, \tag{13}$$

which is also negligible as long as $d \gg \tilde{D}$. The same holds with the *Case 2*. ■

Similar to the conventional definition, we can now define the Fresnel region of LIS. The Fresnel region is given by a distance d_0 such that when d is between d_0 and the Fraunhofer distance, only phase variations are noticeable. This has been observed in [10], and from (13) to have an angle variation $\theta < \pi/8$, d_0 is set to $1.2\tilde{D}$. However, we see from (11) that d_0 has to be at least 4 times large to copy with an instance of the *Case 2*. Therefore, although d_0 is proportional to $\tilde{D}$, it should be set larger, and without loss of generality we define

$$d_0 \triangleq 8\tilde{D}, \tag{14}$$

which is shown latter to be well aligned with numerical tests. On the other hand, when $d < d_0$, it also brings noticeable amplitude and angle variations in addition to the existing phase variations, which is a more challenging task to deal with. However, since d_0 is rather small compared to $d_{F,1}$ or $d_{F,2}$, it happens at a very low chance in practice.

Example 3. *Considering the same configurations as in Example 1 with the Case 1, then $d_0 = 8(N-1)\lambda/\sqrt{2}$ which are about 8.8m and 17.8m for $N = 32$ and 64, respectively. This corresponds to ratios of 18% and 9% of the Fraunhofer distances. Further, as d_0 increases linearly in N, whereas the Fraunhofer distance increases quadratically, the ratio quickly converges to zero as N increases.*

Fig. 2 summarizes what have been discussed so far regarding the definitions of different regions of the LIS.

III. Optimal Near-Field BF for the LIS

As the amplitude and angle variations are negligible, the main objective of the near-field BF is to recover the losses resulted from those phase variations in the Fresnel near-field region. In this section, we derive the optimal near-field BF for a LIS-array, which in principle depends on the location of UE, and in practice can be difficult to obtain. Hence, we propose a near-field BF design with two steps. The first step is to apply a conventional far-field BF to align the boresight of the LIS to the UE, i.e., transferring a UE from the *Case 2* to the *Case 1*. Afterwards, we apply the near-field BF to compensate remaining phase variations with the derived non-DFT beam. The optimal BF in the second step also depends on the distance, however, since in the UE is assumed to be located on the boresight, heuristic approaches can be applied via a code-booked based beam-sweeping and selection, and are simpler than those considered in [6].

A. General Far-field BF

With the far-field BF, the effective channel after Tx and Rx BF can be expressed as

$$h = \xi \boldsymbol{\alpha}(\phi_r, \varphi_r)^\dagger \boldsymbol{\beta}(\phi_r, \varphi_r) \boldsymbol{\beta}(\phi_t, \varphi_t)^\dagger \boldsymbol{\alpha}(\phi_t, \varphi_r), \tag{15}$$

where ξ corresponds to the channel coefficient, and $\boldsymbol{\beta}(\phi_r, \varphi_r)$, $\boldsymbol{\beta}(\phi_t, \varphi_t)$ are steering vectors at the receiver and transmitter sides, respectively. In general, the steering vector $\boldsymbol{\beta}(\phi, \varphi)$ (by omitting the subscripts '*r*' and '*t*') is a DFT beam. With a uniform planar array (UPA) such as the LIS-array depicted in Fig. 1, it can be decomposed into a tensor-product as

$$\boldsymbol{\beta}(\phi, \varphi) = \boldsymbol{\beta}_1(\phi, \varphi) \otimes \boldsymbol{\beta}_2(\phi, \varphi), \tag{16}$$

where ϕ and φ are the azimuth and elevation angles shown in Fig. 1, respectively, and it holds that[2]

$$\boldsymbol{\beta}_1(\phi, \varphi) = (e^{j\pi(M-1)\sin\varphi\cos\phi}, e^{j\pi(M-2)\sin\varphi\cos\phi}, \cdots, 1),$$
$$\boldsymbol{\beta}_2(\phi, \varphi) = (e^{j\pi(N-1)\sin\varphi\sin\phi}, e^{j\pi(N-2)\sin\varphi\sin\phi}, \cdots, 1).$$

The conventional optimal far-field BF vectors $\boldsymbol{\alpha}(\phi_r, \varphi_r)$ and $\boldsymbol{\alpha}(\phi_t, \varphi_t)$ at transmit and receiver sides are then set to

$$\begin{aligned} \boldsymbol{\alpha}(\phi_r, \varphi_r) &= \boldsymbol{\beta}(\phi_r, \varphi_r), \\ \boldsymbol{\alpha}(\phi_t, \varphi_t) &= \boldsymbol{\beta}(\phi_t, \varphi_t). \end{aligned} \tag{17}$$

This yields the highest array-gains that can be harvested. In the Fresnel near-field region, however, the steering vector of the LIS is not of the form $\boldsymbol{\beta}(\phi_t, \varphi_t)$. Rather, it is a vector $\boldsymbol{\gamma}$ comprising of phases $e^{j\epsilon_{mn}}$ depending on the distances d_{mn}. At the UE side, as the receiving antenna-array is typically very small, the phase variations from the LIS to different receiving antennas are negligible, and the steering vector $\boldsymbol{\beta}(\phi_r, \varphi_r)$ and the receiving BF vector $\boldsymbol{\alpha}(\phi_r, \varphi_r)$ remain unaltered as if being in the far-field. After the perfect receiving BF with N_r receiving-antennas, the channel becomes

$$h = \xi N_r \boldsymbol{\gamma}^\dagger \hat{\boldsymbol{\gamma}}. \tag{18}$$

Given (18), our goal is to derive the closed-form of the new steering vector $\boldsymbol{\gamma}$ in the near-field region, and then design the optimal near-field BF vector $\hat{\boldsymbol{\gamma}}$ accordingly. In ideal case,

[2]The steering vectors $\boldsymbol{\beta}_1(\phi, \varphi)$ and $\boldsymbol{\beta}_2(\phi, \varphi)$ are simplified by assuming a $\lambda/2$ antenna-spacing, and the entries are ordered from index 1 to M or N in each dimension, respectively.

when the UE-location is known, a perfect near-field BF can be designed such that $\hat{\boldsymbol{\gamma}}=\boldsymbol{\gamma}$, and $\boldsymbol{\gamma}^{\dagger}\hat{\boldsymbol{\gamma}}=MN$, which yields the highest array-gains. On the other hand, without considering any BF, $\hat{\boldsymbol{\gamma}}$ contains all ones, and it holds that

$$|\boldsymbol{\gamma}^{\dagger}\hat{\boldsymbol{\gamma}}| = \left|\sum_{m,n} e^{j\epsilon_{mn}}\right|, \tag{19}$$

which reflects the array-gain losses. Therefore, $|\boldsymbol{\gamma}^{\dagger}\hat{\boldsymbol{\gamma}}|$ is the array-gain resulting from a given near-field BF vector $\hat{\boldsymbol{\gamma}}$, and can measure the effectiveness of the BF.

B. Formulation of the Near-field BF for Case 1

We start with the *Case-1*, where the distance between the UE and (m,n)th element of the LIS equals

$$d_{mn} = \sqrt{d^2+\Delta_{mn}^2} \approx d + \frac{\Delta_{mn}^2}{2d}, \tag{20}$$

where the condition holds when UE being in the Fresnel region, and Δ_{mn} refers to the distance from the LIS centre to the (m,n)th element which equals

$$\Delta_{mn} = \frac{\lambda}{2}\sqrt{\left(m-\frac{M}{2}-\frac{1}{2}\right)^2+\left(n-\frac{N}{2}-\frac{1}{2}\right)^2}. \tag{21}$$

Then, the phase variation among the received signals emitted by the (m,n)th element can be expressed as

$$\begin{aligned}\epsilon_{mn} &= \frac{2\pi}{\lambda}\frac{\Delta_{mn}^2}{2d} \\ &= \frac{\pi\lambda}{4d}\left(\left(m-\frac{M}{2}-\frac{1}{2}\right)^2+\left(n-\frac{N}{2}-\frac{1}{2}\right)^2\right).\end{aligned} \tag{22}$$

Thusly, the optimal BF needs to compensate these variations on different antenna-elements of the LIS. Further, the phase variation can be decomposed as

$$e^{j\epsilon_{mn}} = e^{j\eta}\cdot e^{j\theta m(m-M-1)}\cdot e^{j\theta n(n-N-1)}, \tag{23}$$

where the variable

$$\theta = \frac{\pi\lambda}{4d}, \tag{24}$$

and

$$\eta = \frac{\pi\lambda}{16d}\left((M+1)^2+(N+1)^2\right). \tag{25}$$

Since the first term $e^{j\eta}$ in (23) is a common factor for all antenna-elements, it can be removed from the BF. The second and the third terms correspond to the optimal weights on the azimuth and elevation directions, respectively. Now we are ready to present the optimal near-field BF in Property 5.

Property 5. *For a LIS of size $M\times N$, the optimal near-field BF vector $\hat{\boldsymbol{\gamma}}$ has the form of $\hat{\boldsymbol{\gamma}}(\theta)=\boldsymbol{\alpha}_1(\theta)\otimes\boldsymbol{\alpha}_2(\theta)$, where the steering vectors $\boldsymbol{\alpha}_1(\theta)$ and $\boldsymbol{\alpha}_2(\theta)$ are of length M and N, respectively, and are equal to*

$$\begin{aligned}\boldsymbol{\alpha}_1(\theta) &= (e^{j\theta M}, e^{j2\theta(M-1)}, \cdots, e^{jm\theta(m-M-1)}, \cdots, e^{j\theta M}), \\ \boldsymbol{\alpha}_2(\theta) &= (e^{j\theta N}, e^{2j\theta(N-1)}, \cdots, e^{-j\theta n(n-M-1)}, \cdots, e^{j\theta N}).\end{aligned} \tag{26}$$

Note that in order to compute the optimal near-field BF vector from Property 5, one still needs to know θ in (24). However, θ only depends on the distance d, rather then the exact UE coordinates, this is a significant simplification for the near-field BF. Further, a codebook based design of θ can be applied.

C. Design of the Near-field BF for Case 2

With the *Case-2*, one needs to compute the distances d_{mn} in (20) directly in order to obtain all phase-variations, which requires knowing the exact UE location. This is a difficult task. In a practical design, we propose to decompose the near-field BF into two steps, which firstly applies an far-field BF to compensate the φ and ϕ as shown in Fig. 1. This step is essentially equivalent to rotate the LIS-array such that the boresight is aligned to the UE location and transfer a general *Case 2* to the *Case 1*. Then in the second step, Property 5 can be utilized for compensating the remaining phases variations.

To be specific, for a UE located at $(x,\, y,\, d)$, it holds that

$$\begin{aligned}\sin\varphi &= \frac{\sqrt{x^2+y^2}}{\sqrt{x^2+y^2+d^2}}, \\ \cos\phi &= \frac{x}{\sqrt{x^2+y^2}}, \\ \sin\phi &= \frac{y}{\sqrt{x^2+y^2}}.\end{aligned} \tag{27}$$

Inserting (27) back into (16) yields the optimal far-field BF design. In practice, a beam-sweeping procedure can be applied, instead of estimating φ and ϕ, to select a suitable beam from a predetermined codebook such as in the fifth-generation new-radio (5G-NR). Then, the second step is to apply the optimal near-field BF with the *Case 1* by setting the distance to $\sqrt{x^2+y^2+d^2}$ in Property 5.

In summary, we propose to set

$$\hat{\boldsymbol{\gamma}} = \boldsymbol{\Gamma}\boldsymbol{\beta}(\phi_t,\varphi_t), \tag{28}$$

where $\boldsymbol{\Gamma}$ is a diagonal matrix comprising of phases $e^{-j\epsilon_{mn}}$, and $\boldsymbol{\beta}(\phi_t,\varphi_t)$ corresponds to a conventional far-field BF such as in (17). The advantage of (28) is that the first step is fully compatible to the existing far-field BF scheme, and the compensation terms $\boldsymbol{\Gamma}$ in the second step can be seen as an additional operation. When the distance is sufficiently large, ϵ_{mn} are all close to 0, and $\boldsymbol{\Gamma}$ becomes an identity matrix, meaning that no near-field BF is needed in the second step since the UE is assumed to be in the far-field.

D. Practical Implementations

Obtaining an accurate estimate for the distance between the UE to the LIS can be difficult. From this aspect, a codebook based near-field BF, can be considered. With which, a pre-defined table of discrete values of θ can be used with a look-up-table (LUT) operation [6], [15]. Through similar approaches such as beam-sweeping or matching, the closet θ from the table can be adopted. The granularity of θ in the LUT operation is subjected to a trade-off between implementation-complexity and attained array-gains.

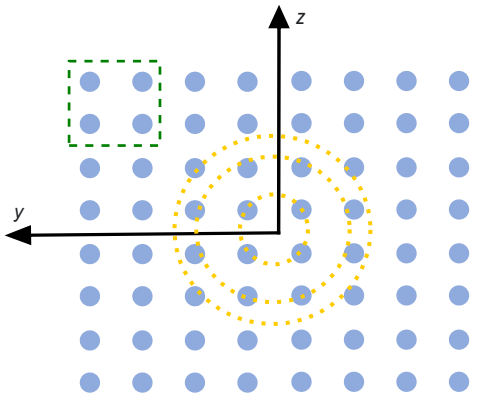

Fig. 3: Antenna-elements on yellow circles have identical phase variations under the *Case 1* and can share a common phase-shift. One can also group adjacent antenna-elements together, e.g., those contained in the green square.

On the other hand, in order to reduce the number of phase-shifts, a group based design of the near-field BF can be adopted. In which case, the LIS-array is split into a number of subgroups, where each subgroup shares a common phase-shift with the same phase adjustment. Note that seen from (26), the near-field beam is symmetric and the number of phase-shifts is half-reduced compared to a DFT beam.

In Fig. 3, we illustrate the grouping based approximations of the near-field BF. Note that the antenna-elements on yellow circles have an identical phase variations with the *Case 1*, and this indicates that a circular shaped array-design could be more efficient for the near-field communication than an UPA. To reduce the number of phase-shifts, one can group antenna-elements contained in a square together for sharing the same phase-shift.

IV. Numerical Results

In this section we present numerical results, and through all tests we set $M=N$ of the LIS-array for simplicity.

A. Optimal Near-field BF

We begin with comparing the beam patterns of the derived near-field beam and a conventional DFT beam with $N=16$, which have the form $e^{j\theta n(n-N-1)}$ and $e^{j\theta n}$, respectively. As seen from Fig. 4, the derived near-field beam is quit different from the DFT beam, and its periodicity is half-reduced to π due to the symmetric from in (26). Further, the side lobes with the near-field beams are much higher than those with the DFT beam, which indicates that the near-field beam could be more robust against distance mismatches.

B. Near-field Regions

Then we show in Fig. 5 an illustration of the near-field and far-field regions. The array-gains $|\boldsymbol{\gamma}^{\dagger}\hat{\boldsymbol{\gamma}}|$ are measured in relation to the distance d with both the *Case 1*, and Example 2 in the *Case 2*. With *Case 1*, a UE is located on the boresight of the LIS, and enters the near-field when $d<d_{F,1}$ which is 48m for λ =5cm and a LIS with $N=32$. This corresponds to a normalized distance in wavelength as $d/\lambda\approx 1000$. When the UE moves away from the boresight as in the Example 2, the Fraunhofer distance $d_{F,2}$ is enlarged by four times from

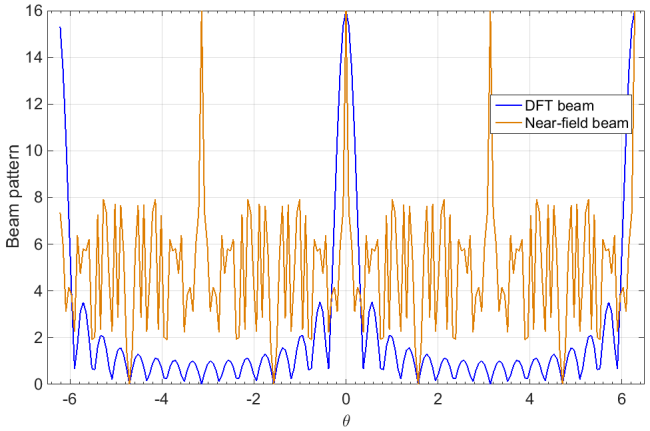

Fig. 4: Beam-patterns of the derived near-field beam and a conventional DFT beam with a 16×16 LIS-array.

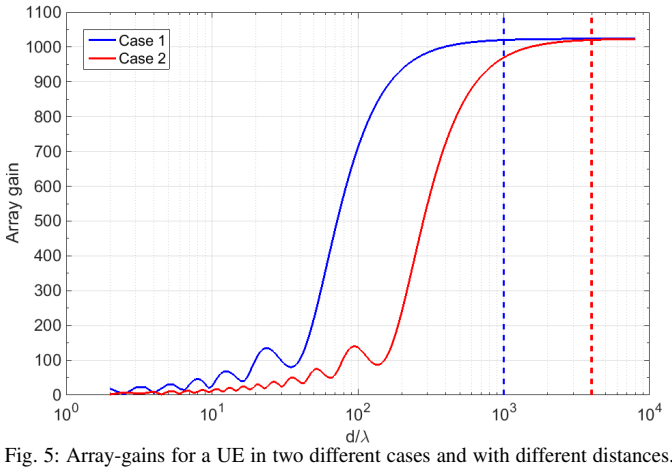

Fig. 5: Array-gains for a UE in two different cases and with different distances.

Property 3, which can also be seen from the figure. These reveal that both Property 1 and Property 3 are well aligned with the numerical results.

C. Optimal Near-field BF

In Fig. 6, the setups are the same as those in Fig. 5, and we use the proposed two-step near-field BF in (28). As seen, the array-gains are improved significantly when the UE enters the Fresnel near-field region, compared to the cases without the near-field BF. Further, we have also simulated the group-based approximations for a 32×32 LIS-array, which is further split into 8 smaller groups of sizes 4×4. In each group, a common phase-shift is applied for the near-field BF. We further considered two different methods. With the method 1, the mean of 16 compensation terms $e^{j\epsilon_{mn}}$ in a group is used for all antenna-elements in the same group, while with the method 2, the mean of 16 distances d_{mn} are used for deriving a common phase ϵ in (22). As seen, both approximations only yield marginal array-gain losses, while method 2 is better than method 1 since the amplitude with method 1 can vary.

Nevertheless, it can also been seen that when d is very small, the near-field BF becomes less effective. This is because $d\gg\lambda$ in (3) does not hold, and both amplitudes and angle variations are not negligible any more. Further, the approximation (20) is also less accurate in this case.

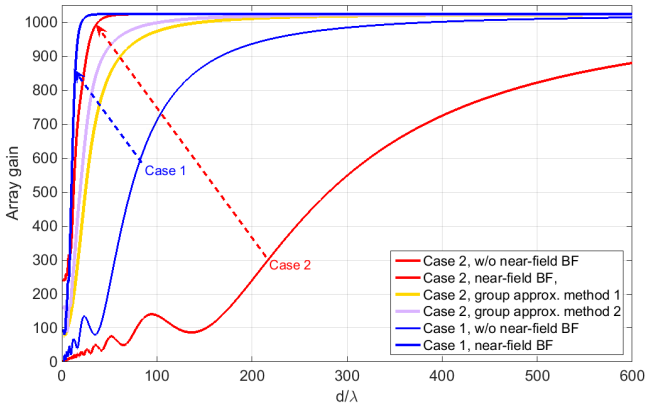

Fig. 6: Array-gain improvements with the proposed near-field BF.

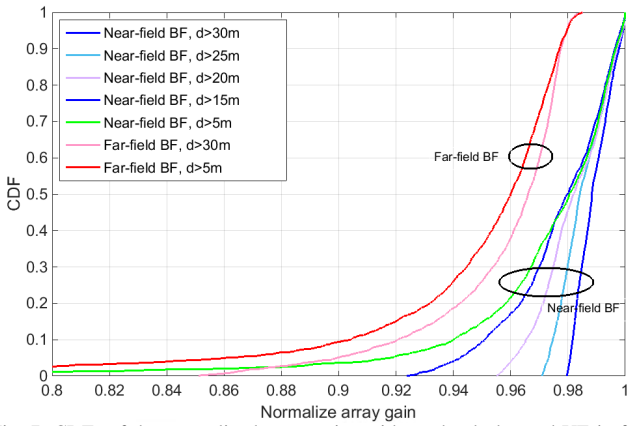

Fig. 7: CDFs of the normalized array-gains with randomly located UE in front of a LIS-array of size 64×64.

In Fig. 7, cumulative probability functions (CDFs) of array-gains with and without the near-field BF are plotted for a 64×64 LIS-array. In this case, $d_{\text{F,1}} = 198$m, and the UE enters the Fresnel near-field region when $d > d_0 = 17.8$m following the definition in (14). We generate 2,000 random locations $(x,\ y,\ d)$ for a single-antenna UE from a uniform distribution in front of the LIS, and satisfy -50m$< x, y <$50m and $d <$50m. Further, to investigate the Fresnel region, we consider different constrains with $d >$5m, 15m, 20m, 25m, and 30m, respectively. As already shown from Fig. 6, the array-gains without the near-field BF are very small and are not shown. We are interested in comparing the cases with only the far-field BF, i.e., the first step in the proposed near-field BF scheme, and with a complete near-field BF with two steps. The intention is to show the improvements of our proposal over a conventional far-field BF that ignores the near-field impacts.

The normalized array-gains are then plotted in Fig. 7, where we see significant gains from the proposed near-field BF. Further, under the case $d > 15$m, the losses are negligible since the main near-field impact is phase variations which can be effectively compensated by the near-field BF. While under the case $d > 5$m, there are noticeable losses. These verify our definition of the Fresnel region in (14), and also show that setting d_0 to $1.2\tilde{D} = 2.7$m in [10] is not sufficiently large. Whereas when the UE is always in the near-field, the far-field BF with the case $d > 30$m yields only marginal gains compared to the case $d > 5$m, since the near-field impacts are ignored.

V. Summary

We have considered the near-field and far-field regions for a LIS, and showed that the Fraunhofer distance scales up linearly in the surface-area of the LIS. Further, we have also derived the Fresnel near-field region of the LIS, where only phase variations worsen the array-gains, but not the amplitude and angles variations. The distance defines the Fresnel regions scales up only linearly in the diameter of the LIS. Enlightened by this observation, we have further derived an optimal near-field BF in the Fresnel near-field region, and proposed a novel scheme that splits the BF into two-steps. The first step applies a conventional far-field BF, while the second step utilizes the derived non-DFT near-field beam to compensate the remaining phases. Practical designs via group based approximations have also been evaluated. The simulation results have shown that the proposed near-field BF scheme can effectively recover the array-gains degraded by the near-field impacts. So far we have only considered a UE with a small antenna-array, while when a UE also receives with a LIS, the near-field impacts at the receiving-LIS should also be considered, which is reciprocal to the transmitting-LIS and can follow similar analysis.

References

[1] I. F. Akyildiz, A. Kak, and S. Nie, "6G and beyond: The future of wireless communications systems," *IEEE Access*, vol. 8, pp. 133995-134030, 2020.

[2] S. Hu, F. Rusek, and O. Edfors, "Beyond massive MIMO: The potential of data transmission with large intelligent surfaces," *IEEE Trans. Signal Process.*, vol. 66, no. 10, pp. 2746-2758, 2018.

[3] S. Hu and F. Rusek, "Spherical large intelligent surfaces," IEEE Int. Conf. Acoust. Speech Signal Process. (ICASSP), Barcelona, Spain, 2020, pp. 8673-8677.

[4] S. Hu, F. Rusek, and O. Edfors, "Beyond Massive MIMO: The potential of positioning with large intelligent surfaces," *IEEE Trans. Signal Process.*, vol. 66, no. 7, pp. 1761-1774, 2018.

[5] Y. Jiang, F. Gao, M. Jian, S. Zhang, and W. Zhang, "Reconfigurable intelligent surface for near field communications: beamforming and sensing," *preprint, arXiv:2204.10114*, 2022.

[6] G. C. Alexandropoulos, V. Jamali, R. Schober, and H. V. Poor, "Near-field hierarchical beam management for RIS-enabled millimeter wave multi-antenna systems," *preprint, arXiv:2203.15557*, 2022

[7] C. Huang et al., "Holographic MIMO surfaces for 6G wireless networks: Opportunities, challenges, and trends," *IEEE Wireless Commun.*, vol. 27, no. 5, pp. 118-125, 2020.

[8] S. Huang, B. Wang, Y. Zhao, and M. Luan, "Near-field RSS-based localization algorithms using reconfigurable intelligent surface," *IEEE Sensors J.*, vol. 22, no. 4, pp. 3493-3505, 2022.

[9] H. Lu and Y. Zeng, "Communicating with extremely large-scale array/surface: unified modelling and performance analysis," *IEEE Trans. Wireless Commun.*, 2021.

[10] E. Björnson, T. Özlem, and L. Sanguinetti, "A primer on near-field beamforming for arrays and reconfigurable intelligent surfaces," *preprint, arXiv:2110.06661*, 2021.

[11] J. G. Ryan and R. A. Goubran, "Near-field beamforming for microphone arrays," IEEE Int. Conf. Acoust. Speech Signal Process. (ICASSP), vol. 1, 1997, pp. 363-366.

[12] M. Cui, L. Dai, R. Schober, and L. Hanzo, "Near-field wideband beamforming for extremely large antenna array," *preprint arXiv:2109.10054*, 2021.

[13] S. Argentieri, P. Danes, and P. Soueres, "Modal analysis based beamforming for near-field or far-field speaker localization in robotics," *IEEE/RSJ Int. Conf. Intel. Robots Syst.*, 2006, pp. 866-871.

[14] H. Lee, W. Ryu, W. Sung, and J. Park, "Beamforming for rotated 3D multipanel array structures for 5G NR MIMO transmission," *Int.l J. Ant. Propag.*, 2019.

[15] M. Cai et al, "Effect of wideband beam squint on codebook design in phased-array wireless systems," IEEE Global Commun. Conf. (GLOBECOM), 2016, pp. 1-6.